



black hole mass in 3C 454.3 to be in the  $10^8$ – $10^{10} M_\odot$  range. The PSD slopes below and above the breaks estimated by Ackermann et al. (2010) and NM13 as well as the location of the PSD breaks were inconsistent with each other which may suggest either a non-stationarity of the variability process in this source, or indeed distinct variability properties of the  $\gamma$ -ray flares.

The methods relying on the PSD extraction require that the light curves are uniformly sampled, or a number of biases are introduced and have to be accounted for, which is not trivial. Models of variability applied directly to the light curves avoid these biases. Kelly et al. (2009, 2011) developed and advocated for stochastic models for luminosity fluctuations of accreting black holes, motivated by PSD proportional to  $1/f^\alpha$  with one or two breaks that have been commonly observed in X-rays in the black hole binaries (e.g. Pottschmidt et al. 2003, Axelsson et al. 2005, Belloni et al. 2005, Reig et al. 2013), and in optical and X-ray bands in AGN (e.g. Markowitz et al. 2003, Kelly et al. 2009). The models of Kelly et al. are based on the Ornstein-Uhlenbeck process or a linear superposition of the OU processes. Thus, they explicitly assume a power-law PSD with one or two characteristic time scales. Kelly et al. derive the likelihood function for their statistical models and perform statistical inference within a Bayesian framework. This allows them to obtain the probability distributions of the model parameters, such as the characteristic time scales and the slopes of the intermediate part of the PSD, given the data. They fully account for the measuring errors, irregular sampling, red noise leak, and aliasing. In addition, direct modeling of the light curves allows to combine easily different sampling time scales. All these advantages make the Kelly et al. models particularly attractive for constraining the PSD of AGN in all energy bands.

In this paper we apply the stochastic models of Kelly et al. to the first 4-year Fermi/LAT light curves of 13 bright blazars. This is the first systematic analysis of the  $\gamma$ -ray blazar light curves in the time domain using the parametric methods which are not sensitive to the observational biases. The paper is organized as follows. In Section 2 we describe the blazar sample and data reduction procedure. The models are summarized in Section 3. In Section 4 we present our results on the derived constraints on the PSD parameters for the sources in our sample. In Section 5 we discuss our findings on the  $\gamma$ -ray blazar variability and perform a comparison with with the X-ray variability properties of blazars and non-blazar AGN. We formulate our conclusions in Section 6.

## 2. FERMI/LAT SAMPLE

We extract  $\gamma$ -ray light curves for a sample of 13 bright blazars using the first 4 years of the publicly available Fermi/LAT data (MJD 54682 – 56143). The sample consists of 8 flat spectrum radio quasar type sources (FSRQ) and 5 BL Lacs (Table 1) that were among the brightest sources in the 2FGL catalog (Nolan et al. 2012) and remained bright during the 3rd and 4th years of the Fermi mission as indicated by the Monitored Source List (e.g., we excluded AO 0235+164). The 100 MeV–300 GeV  $\gamma$ -ray fluxes were calculated in standard unbinned maximum likelihood analysis using the Science Tools software package v9r27p1, instru-

ment response function P7SOURCE\_V6, Galactic diffuse emission model gal\_2yearp7v6.v0, isotropic background model iso\_p7v6source, 10 deg region of interest, and 2FGL-based 15 deg background source model.

Time bins were selected in an adaptive algorithm by dividing each bin (starting from 200 day bins) into equal halves as long as the likelihood analysis for each half satisfied the minimum test statistic criterion  $TS \geq 25$ . The resulting time resolution of the light curves varies in the  $\Delta t \simeq 0.02$ –50 day range. In Figure 1 we plot the relative time of each light curve as a function of the time bin index. In this representation a uniformly binned light curve would be given by a linear relation. It can be seen that the time bin distribution in some light curves (PKS 1510-089, B2 1520+31 and Mrk 421) resembles closely a uniform distribution. On the other hand, light curves of PKS 0454-234, 3C 454, and 3C 273 contain time periods with crude time resolution corresponding to the low flux states of the sources reflected by vertical rises in Figure 1, which separate periods of fine sub-day time resolution associated with the high flux states.

## 3. MODELING

We model the Fermi/LAT light curves of the sources in our sample as a single Ornstein-Uhlenbeck (OU) process (Kelly et al. 2009), or a linear superposition of the OU processes (hereafter sup-OU, Kelly et al. 2011). In this section we summarize briefly the main properties of these processes, and we refer the reader to Kelly et al. (2009, 2011) for the full details of the models construction and fitting procedures.

The OU process,  $X(t)$ , is defined by the following stochastic differential equation:

$$dX(t) = -\omega_0(X(t) - \mu)dt + \varsigma dW(t), \omega_0, \varsigma > 0. \quad (1)$$

The parameters of the process are the characteristic frequency,  $\omega_0$ ; the mean value of the process,  $\mu$ ; and the amplitude of the driving noise process,  $\varsigma$ , being the rate at which variability power is injected into the stochastic process  $X(t)$ . The term  $W(t)$  denotes a Wiener process (i.e., a Brownian motion), and its derivative is white noise. The power spectrum of an OU process is flat for frequencies  $\omega \ll \omega_0$  and decays as  $1/\omega^2$  for frequencies  $\omega \gg \omega_0$ . Hence,  $\omega_0$  may be associated with a characteristic time scale  $\tau_0 = 1/\omega_0$  related with a change in the properties in the PSD of the OU process. The OU process proved to provide an adequate description of the optical light curves of AGN (Kelly et al. 2009; Kozłowski et al. 2010; MacLeod et al. 2010; Zu et al. 2013; Andrae et al. 2013), at least on time scales longer than a  $\sim 3$  months (Mushotzky et al. 2011).

A process defined as a combination of the OU processes,

$$Y_M(t) = \mu + \sum_{i=1}^M c_i X_i(t), \quad (2)$$

where  $c_1, \dots, c_M$  is a set of mixing weights, and  $X_1(t), \dots, X_M(t)$  is a set of the OU processes, allows to model light curves with more complex PSD, e.g. those that are flat below a low-frequency break,  $\omega_1$ , decay as  $1/\omega^\alpha$  with  $\alpha = 0$ –2 above the low-frequency break, and then steepen to  $1/\omega^2$  above a high-frequency break,  $\omega_2$ , as observed e.g. in the X-ray PSD of nearby AGN and black hole

X-ray binaries (e.g. Kelly et al. 2011, Axelsson et al. 2005). We define the short and long term characteristic time scales related to the two characteristic frequencies as  $\tau_S = 1/\omega_2$  and  $\tau_L = 1/\omega_1$ . The characteristic time scales that we sample for are between  $\tau_{\max}$  and  $\tau_{\min}$  chosen to be 100 (10) times the length of the time series, and one-hundredth (one-tenth) the smallest time spacing in the time series in the OU (sup-OU) model. Throughout the paper it holds that a Fourier frequency  $f = t^{-1} = \omega/2\pi = (2\pi\tau)^{-1}$ , where  $t$  is a specific time scale. Thus, our study covers a wide range of characteristic time scales corresponding to the  $f \simeq 10^{-11}$ – $10^{-3}$  Hz and  $f \simeq 10^{-10}$ – $10^{-4}$  Hz range in Fourier frequency in the OU and sup-OU models, respectively.

Uttley et al. (2005) argued that the X-ray light curves of X-ray binaries and AGN,  $x(t)$ , are formally non-linear, and can be described by the simple transformation  $x(t) = \exp[l(t)]$ , where  $l(t)$  is a linear, Gaussian time series. The observational evidence supporting this conclusion include the linear rms-flux relation observed on all time scales in the X-ray variations of GBHs and AGNs (Uttley & McHardy 2001), and the log-normal distribution of fluxes for Cygnus X-1 (Uttley et al. 2005). Thus, we model the natural logarithm of the Fermi/LAT fluxes in order to investigate whether the  $\gamma$ -ray light curves of AGN share the properties of the optical and X-ray AGN light curves.

The error bars derived in this work are representative of the 90% confidence regions, while the upper and lower limits represent the 99% confidence regions. While reporting the results, we use logarithms to base 10 and calculate time scales in the observer’s frame, unless otherwise stated.

## 4. RESULTS

### 4.1. The OU process

First, we modeled the Fermi/LAT light curves of the blazars in our sample with the OU process. We plot the light curves, the model realizations corresponding to the highest posterior likelihood, the standardized model residuals and their histograms compared to the expected standard normal distribution in Figures 2–6 (left). The sample posterior distribution functions of the characteristic time scale,  $\tau_0$  are presented in Figure 7. In Table 1 we list the median characteristic time scales and their uncertainties for all sources. The OU modeling gives the characteristic time scales in the  $\tau_0 \simeq 0.7$ –43 day range (Table 1). In the case of 3C 454.3 the characteristic time scale is not constrained, and we derive the lower limit on its value,  $\log[\tau_0/\text{day}] > 2.0$ .

It is apparent that in general the OU process does not fit well the studied light curves. In particular, the model experiences systematic difficulties to fit the data during the quiet time periods when the assumed condition that  $\text{TS} \geq 25$  forces the adaptive time bins  $\Delta t$  to be larger than a few days (see e.g. Figures 3–5, left). To evaluate the quality of the fits, we compare the distributions of the standardized fit residuals with the standard normal distribution. In addition for each source we calculate the auto-correlation function of the standardized residuals (Figure 8). It can be observed that while the distribution of the residuals approximate the standard normal distribution reasonably well, the auto-correlation functions deviate in several sources (e.g. B2 1633+38) from

that expected for the white noise process. Thus, we proceed to testing the sup-OU model on the Fermi/LAT light curves of blazars.

### 4.2. The sup-OU process

In the next step we considered the superposition of the OU processes (sup-OU) and applied it to the Fermi/LAT blazar light curves. We observed a significant improvement to the quality of the fits in the low-flux periods, compared to the case of the OU modeling. The distributions of the standardized residuals assuming the sup-OU process can be compared with the OU model fit residuals and the standard normal distribution (Figures 3–6, right). The auto-correlation functions of the standardized residuals assuming the sup-OU process indicate that, indeed, in majority of sources the sup-OU residuals approximate the white noise process better than the OU process residuals (Figure 8).

To evaluate formally what model is more successful in describing the Fermi/LAT blazar light curves, we computed the deviance information criterion (DIC, Spiegelhalter et al. 2002). DIC is used in Bayesian model selection problems where the posterior distributions of the models have been obtained by Markov chain Monte Carlo simulations. Models with smaller DIC are preferred to models with larger DIC. It is accepted that  $\Delta(\text{DIC}) \gtrsim 10$  is a difference substantial enough to prefer the model with smaller DIC. We use the following definition of the DIC.

$$\text{DIC} = p_V + \bar{D}, \quad (3)$$

where  $p_V = 0.5 \times \text{Var}[D(\theta)]$  describes the effective number of model parameters and hence the model complexity; while  $D(\theta)$  is the deviance defined as  $D(\theta) = -2 \log[p(y|\theta)]$ , where  $p(y|\theta)$  is the model likelihood function,  $y$  are the data, and  $\theta$  denotes the parameters in the model. The second term in Equation 3,  $\bar{D}$ , is the expected value of the deviance.

The comparison of DIC computed for the two models (Table 1) indicates that the sup-OU model is preferred over the OU model in all sources except 3C 454.3, 3C 66A, and PKS 2155-304 in which  $\Delta\text{DIC} = \text{DIC}_{\text{supOU}} - \text{DIC}_{\text{OU}} < 10$ . Thus, for these three sources we accept the results of the OU modeling, while for the remaining sources we assume the results of the sup-OU modeling.

For each source, we plot the posterior probability distributions of the short and long characteristic time scales resulting from the sup-OU model in Figure 9. We notice that in many cases the posterior probability distributions of the characteristic time scales deviate from a Gaussian distribution. It can be inferred that while formally we can derive the median long and short characteristic time scales and their 90% confidence intervals in all sources, they may depend on our choice of  $\tau_{\min}$  and  $\tau_{\max}$ . The least deviated shapes are those representing the long characteristic time scale in PKS 1510-089; and the short characteristic time scales in 3C 454.3, and (to a lesser degree) in 3C 66A, PKS 0716+714, and BL Lac. Thus, we provide the median  $\tau_L$  and/or  $\tau_S$  and their uncertainties for these five cases, and the relevant limits for all sources (Table 1). The upper limits on  $\tau_S$  can be compared with the smallest time spacing in the respective light curves,  $\Delta t$  (see Table 1), and the shortest sampled time scale,  $\tau_{\min} = \Delta t/10$ .

We present the posterior probability distributions of the slopes,  $\alpha$ , characterizing the intermediate part of the PSD between  $\tau_L$  and  $\tau_S$  in Figure 10. The distributions peak close to  $\alpha \simeq 1$  for the majority of the sources. The individual values and their uncertainties are listed in Table 1. The slopes do not depend on the blazar class (BL Lac vs. FSRQ) or redshift (Figure 11, right; left). With the sup-OU model, we constrain the PSD slopes in all sources, except 3C 454.3 for which we find  $\alpha < 0.43$ .

## 5. DISCUSSION

We analyzed the variability properties of 13 bright blazars with the most complete first 4-year Fermi/LAT light curves available from the satellite archive. We used the stochastic models for luminosity fluctuations developed in Kelly et al. (2009, 2011). The models rely on computing the likelihood function and performing Bayesian inference to access the probability distributions of the variability parameters such as, e.g., the characteristic time scales, given the data. The models implement the OU (Ornstein-Uhlenbeck) process leading to a bending PSD, and the superposition of the OU processes leading to a doubly bent PSD. These shapes of PSD are typically observed in radio-quiet AGN in the optical and X-ray bands, and in X-rays in the black hole binaries across different spectral states. Our approach provides an alternative to the methods relying on the PSD extraction known to suffer from a number of observational biases due to irregular sampling, read noise leak, and aliasing. Moreover, our approach allows for non-uniform binning of the light curves. Hence, in this work we binned the light curves adaptively in order to avoid compromising the time resolution in high flux periods for the sake of uniform binning over the entire observing period. In addition, in our modeling we sampled a wide range of temporal frequencies, up to 8 orders of magnitude starting at  $f_{\min} \simeq 10^{-11}$ – $10^{-10}$  Hz. Thus, we improved significantly over the earlier Fermi/LAT blazar variability studies (e.g.,  $f \simeq 0.003$ – $0.2$  Hz, Abdo et al. 2010;  $f \simeq 10^{-7}$ – $10^{-5}$  Hz, NM13).

### 5.1. Characteristic time scales in blazars

The main result of our study is the consistency of the 4-year Fermi/LAT blazar activity with stochastic processes. The mixed OU process was preferred in 10 blazars from our sample, while in the 3 remaining blazars (two BL Lacs, 3C 66A and PKS 2155-304; and one FSRQ 3C 454.3) the single OU process and the mixed OU process resulted in fits of equally good quality.

The posterior probability distributions of the characteristic time scales from the OU process allowed us to constrain the Fermi/LAT characteristic time scales in two BL Lac sources ( $\log[\tau_0/\text{day}] = 1.39_{-0.29}^{+0.43}$  in 3C 66A, and  $\log[\tau_0/\text{day}] = 1.63_{-0.35}^{+2.79}$  in PKS 2155-304). This is the first time that the characteristic time scales have been observed in the Fermi/LAT light curves of blazars other than 3C 454.3. In 3C 454.3 the OU modeling resulted only in a lower limit,  $\log[\tau_0/\text{day}] > 2.0$ , which was inconsistent with the NM13 result. NM13 found that the PSD of 3C 454.3 can be characterized with  $\alpha \simeq 1$  and  $\alpha \simeq 3$  below and above the PSD break, respectively. The high frequency slope significantly steeper than  $\sim 2$  assumed in our modeling might have led to poor constraints on the

characteristic time scales in this source. Characteristic time scales found through the OU modeling in 3C 66A and PKS 2155-304 fall outside of the frequency range studied by NM13. We conclude that perhaps the method of the PSD construction used by NM13 was not sensitive enough to detect these BL Lac characteristic time scales in the Fermi/LAT light curves.

With regard to the sup-OU modeling, we reported the relevant limits on the characteristic time scales. In five cases with the posterior probability distributions resembling most closely a Gaussian distribution ( $\tau_S$  in 3C 454.3, 3C 66A, PKS 0716+714, and BL Lac;  $\tau_L$  in PKS 1510-089) we provided additionally the median values and their uncertainties. However, we cautioned that they might be affected by our choice of the lowest and highest sampled time scales,  $\tau_{\min}$  and  $\tau_{\max}$ . The upper limits on the short characteristic time scales obtained in our studies hint toward a sub-hour  $\gamma$ -ray time variability in at least 4 blazars: B2 1633+38, B2 1520+31, PKS 0454-234, and 3C 273, all belonging to the FSRQ class (Figure 11, left). Sub-hour variability time scales have been reported previously in another FSRQ, PKS 1510-089, in the context of the  $\gamma$ -ray flux doubling/halving time scales, rather than the characteristic time scales, in the study of the  $\gamma$ -ray flares in this source (Saito et al. 2013). Our adaptive light curves do not sample the sub-hour time scales due to a conservative TS constraint in each time bin. However, even with less constraining condition on TS it would be difficult to obtain sub-hour time resolution for a prolonged time required by our study, given the variable nature of blazars, as well as the characteristics of the Fermi/LAT instrument. Obtaining sub-hour time resolution in the Fermi/LAT light curves is feasible only for the highest  $\gamma$ -ray flux periods observed in the  $\gamma$ -rays. Yet, the results might be affected by the poorly understood systematic errors related to the Fermi/LAT data analysis on sub-orbital time scales. The lower limits on the long characteristic time scales indicate that observations conducted for a period of time longer than 4 years considered here are needed in order to constrain  $\tau_L$ .

Ackermann et al. (2010) computed a PSD and structure function of a 120 day long section of Fermi/LAT light curve of 3C 454.3, during which a powerful flare was recorded (MJD 55,120–55,260). They reported a 6.5 day time scale for this time period. We tested our models on the light curve of 3C 454.3 spanning the same range in MJD. Both the OU and sup-OU models resulted in fits of comparable quality ( $\Delta\text{DIC} \simeq 3$ ). However, the  $\tau_S$  and  $\tau_L$  distributions obtained through the sup-OU modeling were poorly separated indicating at most a presence of one characteristic time scale in the light curve. The OU modeling was not successful in constraining the time scale and we obtained only a lower limit,  $\log[\tau_0/\text{day}] > 1.0$ . The OU limit on  $\tau_0$  derived for the 120 day light curve of 3C 454.3 and the 6.5 day time scale reported in Ackermann et al. (2010) are in disagreement, most probably due to the difference between the PSD assumed in the OU model and that found in Ackermann et al. (2010;  $\alpha \simeq 1.40$  and  $\alpha \simeq 1.56$  below and above the PSD break, respectively).

### 5.2. Blazar PSD slopes

In 10 of 13 Fermi/LAT blazar light curves in our sample the sup-OU model was preferred over the OU model

based on DIC. Thus, the second important result of our study is that for the range of time scales sampled with the sup-OU model (Figure 11, left), the underlying PSD of these 10 sources resemble a power-law function proportional to  $1/f^\alpha$  with  $0 < \alpha < 2$ , with majority of the slopes clustering around unity (Figure 10). We were able to constrain the slopes  $\alpha$  in all but one source, 3C 454.3, for which we found  $\alpha < 0.43$ .

Abdo et al. (2010) reported on an average Fermi/LAT PSD slope for their brightest FSRQs,  $\alpha_{\text{FSRQ}} = 1.5 \pm 0.2$ , and BL Lac's,  $\alpha_{\text{FSRQ}} = 1.7 \pm 0.3$ . In general, the slopes derived for the individual sources in our sample through the sup-OU modeling are shallower than those respective averages. In the FSRQ class, slopes of all our sources are inconsistent with the Abdo et al. average. In the BL Lac class, only PKS 2155-304 and (marginally) BL Lac and Mkn 421 have the slopes consistent with the Abdo et al. average at the  $2\sigma$  confidence level, but these are the three source with the broadest posterior slope distributions in our sample (see Figure 10).

We also compared our derived PSD slopes to those found by NM13 (Table 1). We found that in PKS 0454-234, 3C 279, 3C 66A, and PKS 2155-304 the two methods are consistent with each other in terms of the derived PSD slopes within the provided error bars. In 3C 454.3, PKS 1510-089, 3C 273, BL Lac and Mkn 421 our slopes were shallower than those derived by NM13. In 3C 454.3 we suspect that the reason for the discrepancy is in our assumption that the high frequency slope equals 2. If this slope is as steep as 3 reported in NM13 then our modeling might result in a slope below the high frequency break that is flatter than the actual value in order to maintain a satisfactory fit.

### 5.3. Models of blazar variability

The origin of blazar  $\gamma$ -ray variability seen in the Fermi/LAT light curves remains under discussion. In our studies, we followed a stochastic approach to describe this variability motivated by its success in explaining the optical and/or X-ray variability of non-blazar accreting black holes. We demonstrated that the OU and/or mixed OU processes approximate well the blazar  $\gamma$ -ray light curves. Our modeling implies non-linearity of these blazar light curves, similarly to the case of the black hole binary and AGN X-ray light curves, as argued by Uttley et al. (2005).

The interpretation of our models with regard to the optical and/or X-ray black hole variability is along the line of the propagation class of models (e.g. Lyubarskii 1997, Kotov et al. 2001) where perturbations originating at outer radii of an accretion disk propagate inwards and couple with each other producing the observed broad PSD shapes. In particular, Kelly et al. (2011) showed that the mixed OU process is the solution to the linear diffusion equation perturbed by a spatially correlated noise field. Within this framework the low-frequency break in the PSD corresponds to the diffusion time scale in the outer region of the accretion flow, and the shape of the PSD above the low-frequency break depends on the viscosity of the flow. An additional high-frequency break in the PSD may exist if the noise field is spatially correlated. The high-frequency break corresponds then to the time it takes a perturbation traveling at the viscous speed to cross the characteristic spatial scale of the

noise field.

The short characteristic time scale corresponding to the high-frequency break in the black hole binary and AGN X-ray PSD is an important variability parameter due to its correlation with the black hole mass and mass accretion rate that holds over many orders of magnitude (McHardy et al. 2006, Kelly et al. 2011). Kelly et al. (2011) demonstrated that  $\tau_S$  obtained through direct modeling of the 2–10 keV X-ray light curves of a sample of 10 nearby Seyfert galaxies (Sobolewska & Papadakis 2009) with the sup-OU process are in agreement with those derived using the PSD construction methods (Markowitz et al. 2003, McHardy et al. 2007, González-Martín & Vaughan 2012). However, blazar  $\gamma$ -ray emission is dominated by the processes related to the jet physics and beamed due to relativistic effects, unlike the X-ray coronal emission of the radio-quiet AGN and black hole binaries. Nevertheless, it could be envisaged that the accretion disk variability structure is carried outwards in the jet, leading to the jet variability with properties inherited from the innermost radii of the accretion disk/X-ray corona system (e.g. Lohfink et al. 2013). It would be then expected that the X-ray and Fermi/LAT short characteristic time scales of blazars were consistent with those found in X-rays in radio-quiet and radio-loud AGN. Thus, it is interesting to compare the blazar and non-blazar variability properties across different energy bands in order to search for evidence in favor or against a common variability mechanism (Figure 11, middle; note differing frequency bands sampled by the respective studies).

Blazar PSD have been studied in only several sources in energy bands other than the  $\gamma$ -rays. Soft X-ray blazar PSD (here below 20 keV) were computed for three BL Lac sources (Mkn 421 and PKS 2155-304 also included in our Fermi/LAT sample, and Mkn 501) by Kataoka et al. (2001), and for FSRQ sources by McHardy (2008; 3C 273), Chatterjee et al. (2008; 3C 279). Characteristic time scales corresponding to the high-frequency PSD break were detected in all of these sources with the exception of 3C 279. The sampled frequency bands and detected PSD breaks are indicated in Figure 11 (middle). In general, these studies demonstrated that in soft X-rays blazars show high-frequency breaks and PSD shapes below these breaks that are largely consistent with those of Seyfert galaxies and radio-loud AGN (e.g. 3C 120, Marshall et al. 2009; 3C 390.3, Gliozzi et al. 2009), despite a possible contribution from a jet emission in the latter class. However, at the frequencies above the high-frequency break the soft X-ray PSD of BL Lacs seem to drop more rapidly than it is observed in Seyfert galaxies. Hard X-ray (14–150 keV; Swift/BAT) PSD have been recently constructed by Shimizu & Mushotzky (2013) for a sample of 30 AGN, which included two FSRQs (3C 273 and 3C 454.3) and one BL Lac (Mkn 421). This study covered longer time scales than the soft X-ray study of Kataoka et al. (2001). A characteristic time scale was detected only in 3C 273 preventing a detailed cross-band comparison. The PSD of all other AGN in their sample were described with unbroken power-law functions with a typical slopes,  $0 < \alpha < 2$ , when constrained.

The  $\gamma$ -ray blazar PSD slopes derived in our study are in general consistent with those observed in X-rays in non-blazar AGN. However, we were able to derive only

the upper limits on the blazar short characteristic time scales. Given that they are consistent with the low end of  $\tau_S$  detected in the radio-quiet AGN (Figure 11), we cannot discard the possibility that the  $\gamma$ -ray  $\tau_S$  in blazars and the X-ray  $\tau_S$  in non-blazar AGN are comparable.

However, the OU  $\gamma$ -ray characteristic time scales detected in PKS 2155-304 and 3C 66A are much longer than those of the BL Lac sources (and also FSRQs) in the soft X-rays. In addition, closer inspection of few available blazar PSD across different energy bands suggests that they are rather different. In particular, in PKS 2155-304 the value on  $\tau_S$  derived in our work is in disagreement with the X-ray  $\tau_S$  found in Kataoka et al. (2001). The PSD slope derived here for 3C 279,  $\alpha \simeq 1.1$ , is in disagreement with that reported in the soft X-rays by Chatterjee et al. (2008,  $\alpha \simeq 2.3$ ). We do not detect a  $\gamma$ -ray characteristic time scale in 3C 273, while the soft and hard X-ray detections were reported at the values well within our range of sampled time scales (McHardy 2008, Shimitzu & Mushotzky 2013). These discrepancies imply that either the blazar variability process is energy dependent, or the origins of the X-ray and  $\gamma$ -ray blazar variability are different.

The processes intrinsic to the jet physics such as the internal shock model (e.g. Ghisellini 1999) or the minijets-in-a-jet model (e.g. Begelman et al. 2008, Giannios et al. 2009, Narayan & Piran 2012) may well dominate the blazar variability structure leading to the  $\gamma$ -ray variability properties that are largely different from those implied by the accretion disk physics and propagation models. Alternatively, the  $\gamma$ -ray variability pattern may be a combination of the baseline stochastic disk/corona variability carried out in a jet, and variability intrinsic to the jet. If the propagation model of variability envisaging coupling of perturbations at different radii continues toward the jet, and the disk X-ray perturbations couple with the X/ $\gamma$ -ray perturbations intrinsic to the jet, then the resulting Fermi/LAT variability structure may differ from that known from the X-ray band. Additional complication may be introduced by altering the variability time scales due to relativistic effects.

## 6. CONCLUSIONS

We have applied the stochastic models of luminosity fluctuations developed in Kelly et al. (2009, 2011) to the Fermi/LAT light curves of 13 well observed blazars in order to study their time variability properties. The

light curves of 3 blazars were consistent with the OU process which is characterized with a PSD  $\propto 1/f^\alpha$  featuring a bend at a characteristic times scale,  $\tau_0$ , where the slope,  $\alpha$ , changes from 0 ( $\tau \gg \tau_0$ ) to 2 ( $\tau \ll \tau_0$ ). We constrained  $\tau_0$  in two BL Lac type blazars, 3C 66A ( $\tau_0 \simeq 25$  day, or  $\simeq 17$  day in the rest frame) and PKS 2155-304 ( $\tau_0 \simeq 43$  day, or  $\simeq 38$  day in the rest frame). Thus, the inferred  $\gamma$ -ray BL Lac characteristic time scales were longer than those observed in the soft X-ray blazar and Seyfert light curves. In addition, the low- and high-frequency PSD slopes in the BL Lacs fitted well with the OU process were flatter than their counterparts in the soft X-rays. These discrepancies indicate either the energy dependence of the PSD or different origins of the BL Lac X-ray and  $\gamma$ -ray variability.

In 10 of 13 sources a better agreement with the data was obtained with the mixed OU process characterized with a PSD featuring two bends and an intermediate part of PSD where  $0 < \alpha < 2$ . For these sources we derived respective limits on the long and short characteristic time scales. We concluded that their underlying PSD has likely the form of a power-law function over the sampled range of temporal frequencies. The upper limit on the short characteristic time scale indicates sub-hour variability in 4 FSRQ sources. This finding needs to be addressed by present and future theoretical models of blazar  $\gamma$ -ray variability. We constrained the PSD slopes,  $\alpha$ , for all sources except 3C 454.3.

Our stochastic approach is particularly well suited for the variability studies of various classes of AGN because it accounts self-consistently for irregular sampling, measurement errors, red noise leak, and aliasing. Thus, it provides an alternative to the variability methods based on the PSD construction.

This research made use of data obtained with the Fermi Gamma-Ray Observatory. The authors thank Mitch Begelman and James Chiang for discussions and comments. Partial support for this work was provided by the Fermi grant NNX11AO45G and by NASA contract NAS8-03060. M.A.S. was partially supported by the Polish National Science Center grant No. 2011/03/B/ST9/03281. K.N. was supported by NASA through Einstein Postdoctoral Fellowship grant No. PF3-140112 awarded by the Chandra X-ray Center, which is operated by the Smithsonian Astrophysical Observatory for NASA under contract NAS8-03060.

## REFERENCES

- Abdo, A. A., Ackermann, M., Ajello, M., et al. 2010, *ApJ*, 722, 520  
 Ackermann, M., Ajello, M., Baldini, L., et al. 2010, *ApJ*, 721, 1383  
 Andrae, R., Kim, D.-W., & Bailer-Jones, C. A. L. 2013, *A&A*, 554, A137  
 Axelsson, M., Borgonovo, L., & Larsson, S. 2005, *A&A*, 438, 999  
 Begelman, M. C., Fabian, A. C., & Rees, M. J. 2008, *MNRAS*, 384, L19  
 Belloni, T., Homan, J., Casella, P., et al. 2005, *A&A*, 440, 207  
 Chatterjee, R., Jorstad, S. G., Marscher, A. P., et al. 2008, *ApJ*, 689, 79  
 Ghisellini, G. 1999, *Astronomische Nachrichten*, 320, 232  
 Giannios, D., Uzdensky, D. A., & Begelman, M. C. 2009, *MNRAS*, 395, L29  
 Glozzi, M., Papadakis, I. E., Eracleous, M., et al. 2009, *ApJ*, 703, 1021  
 González-Martín, O., & Vaughan, S. 2012, *A&A*, 544, A80  
 Kataoka, J., Takahashi, T., Wagner, S. J., et al. 2001, *ApJ*, 560, 659  
 Kelly, B. C., Bechtold, J., & Siemiginowska, A. 2009, *ApJ*, 698, 895  
 Kelly, B. C., Sobolewska, M., & Siemiginowska, A. 2011, *ApJ*, 730, 52  
 Kotov, O., Churazov, E., & Gilfanov, M. 2001, *MNRAS*, 327, 799  
 Kozłowski, S., Kochanek, C. S., Udalski, A., et al. 2010, *ApJ*, 708, 927  
 Lohfink, A. M., Reynolds, C. S., Jorstad, S. G., et al. 2013, *ApJ*, 772, 83  
 Lyubarskii, Y. E. 1997, *MNRAS*, 292, 679  
 MacLeod, C. L., Ivezić, Ž., Kochanek, C. S., et al. 2010, *ApJ*, 721, 1014  
 Marshall, K., Ryle, W. T., Miller, H. R., et al. 2009, *ApJ*, 696, 601

TABLE 1  
PROPERTIES OF THE FERMI/LAT BLAZAR LIGHT CURVES.

Name	$z$	$\log \tau_0$	DIC	$\alpha$	$\alpha_{\text{NM13}}$	$\log \tau_S$	$\log \Delta t$	$\log \tau_L$	DIC		
		(1)	(2)	(3)	(4)	(5)	(6)	(7)	(8)	(9)	(10)
FSRQs											
B2 1633+38	1.814	$-0.13^{+0.12}_{-0.12}$	1871	$1.00^{+0.06}_{-0.06}$	-	$< -1.53$	-1.3	$> 2.27$	1663		
PKS 1424-41	1.522	$0.75^{+0.14}_{-0.12}$	1315	$0.78^{+0.10}_{-0.09}$	-	$< -0.87$	-1.4	$> 2.06$	1222		
B2 1520+31	1.487	$-0.01^{+0.08}_{-0.08}$	2458	$1.05^{+0.08}_{-0.07}$	-	$< -1.35$	-1.3	$> 2.00$	2301		
PKS 0454-234	1.003	$0.25^{+0.11}_{-0.11}$	1733	$0.93^{+0.08}_{-0.07}$	$0.777 \pm 0.274$	$< -1.26$	-1.3	$> 2.44$	1578		
3C 454.3	0.859	$> 2.00$	254	$< 0.43$	$0.999 \pm 0.235$	$0.32^{+1.47}_{-1.22}$	$< 3.21$	-0.6	$> 2.53$	250	
3C 279	0.536	$-0.01^{+0.09}_{-0.09}$	2425	$1.03^{+0.06}_{-0.06}$	$1.078 \pm 0.246$	$< -1.53$	-1.3	$> 2.39$	2169		
PKS 1510-089	0.360	$1.03^{+0.11}_{-0.10}$	1386	$0.48^{+0.19}_{-0.20}$	$1.101 \pm 0.298$	$< -0.16$	-0.6	$2.17^{+1.52}_{-0.45}$	$> 1.64$	1350	
3C 273	0.158	$0.38^{+0.10}_{-0.10}$	1509	$0.84^{+0.11}_{-0.09}$	$1.301 \pm 0.265$	$< -1.03$	-1.6	$> 2.06$	1408		
BL Lacs											
3C 66A	0.444	$1.39^{+0.43}_{-0.29}$	448	$0.81^{+0.50}_{-0.44}$	$0.604 \pm 0.438$	$-0.03^{+0.76}_{-1.19}$	$< 1.03$	-0.7	$> 1.87$	445	
PKS 0716+714	0.300	$0.17^{+0.10}_{-0.10}$	1941	$1.05^{+0.20}_{-0.16}$	-	$-1.10^{+0.44}_{-0.73}$	$< -0.53$	-1.3	$> 1.82$	1876	
PKS 2155-304	0.116	$1.63^{+2.79}_{-0.35}$	477	$0.64^{+0.79}_{-0.50}$	$0.577 \pm 0.332$	$< 1.61$	-0.7	$> 1.70$	468		
BL Lac	0.069	$0.47^{+0.15}_{-0.15}$	865	$0.93^{+0.18}_{-0.14}$	$0.412 \pm 0.469$	$-1.16^{+0.52}_{-0.72}$	$< -0.46$	-1.3	$> 2.11$	811	
Mkn 421	0.030	$0.82^{+0.13}_{-0.13}$	1351	$0.94^{+0.13}_{-0.13}$	$0.384 \pm 0.205$	$< -0.51$	-0.8	$> 1.78$	1306		

**Notes:** All characteristic time scales are reported in days and in the observer's frame. (1) Characteristic time scale of the OU process,  $\tau_0$ , in days. (2/10) Deviance Information Criterion, DIC, for the OU/sup-OU model; models with smaller DIC are preferred. (3) Slope of the PSD  $\propto 1/f^\alpha$  between the short and long characteristic time scales in the sup-OU model (90% confidence region). (4) Slope of the PSD  $\propto 1/f^\alpha$  derived by NM13 through the Fermi/LAT PSD construction. (5) Short characteristic time scale in the sup-OU model,  $\tau_S$ , in days (90% confidence region). (6) Upper limits on the short characteristic time scale in the sup-OU model (99% confidence region). (7) The smallest time spacing in the light curve,  $\Delta t$ , in days. (8) Long characteristic time scale in the sup-OU model,  $\tau_L$ , in days (90% confidence region). (9) Lower limit on the long characteristic time scale in the sup-OU model (99% confidence region).

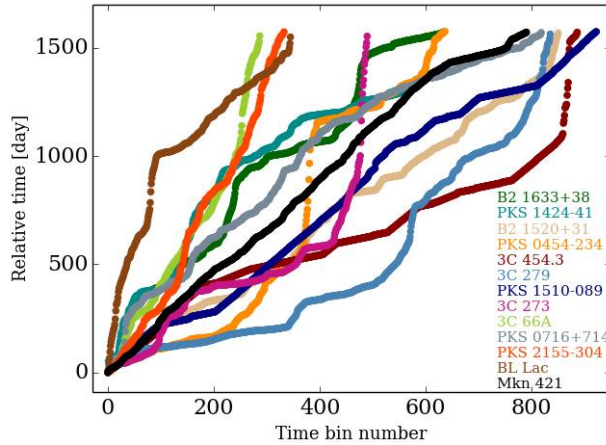


FIG. 1.— Relative time as a function of the time bin number. The time bin sizes are in the  $\Delta t \simeq 0.02$ –50 day range. The time resolution of several light curves is close to uniform. Other light curves contain periods with crude time resolution corresponding to the low flux states (vertical rises), which separate fine time resolution periods with high flux.

- McHardy, I. M., Koerding, E., Knigge, C., Uttley, P., & Fender, R. P. 2006, *Nature*, 444, 730
- McHardy, I. M., Arévalo, P., Uttley, P., et al. 2007, *MNRAS*, 382, 985
- McHardy, I. 2008, *Blazar Variability across the Electromagnetic Spectrum*, published online at <http://pos.sissa.it>
- Markowitz, A., Edelson, R., Vaughan, S., et al. 2003, *ApJ*, 593, 96
- Mushotzky, R. F., Edelson, R., Baumgartner, W., & Gandhi, P. 2011, *ApJ*, 743, L12
- Nakagawa, K., & Mori, M. 2013, *ApJ*, 773, 177
- Nalewajko, K. 2013, *MNRAS*, 430, 1324
- Narayan, R., & Piran, T. 2012, *MNRAS*, 420, 604
- Nolan, P. L., Abdo, A. A., Ackermann, M., et al. 2012, *ApJS*, 199, 31
- Pottschmidt, K., Wilms, J., Nowak, M. A., et al. 2003, *A&A*, 407, 1039
- Reig, P., Papadakis, I. E., Sobolewska, M. A., & Malzac, J. 2013, *MNRAS*, 435, 3395
- Shimizu, T. T., & Mushotzky, R. F. 2013, *ApJ*, 770, 60
- Sobolewska, M. A., & Papadakis, I. E. 2009, *MNRAS*, 399, 1597
- Spiegelhalter, D. J., Best, N. G., Carlin, B. P., & Van Der Linde, A. 2002, *Journal of the Royal Statistical Society: Series B (Statistical Methodology)*, 64, 583
- Uttley, P., & McHardy, I. M. 2001, *MNRAS*, 323, L26
- Uttley, P., McHardy, I. M., & Vaughan, S. 2005, *MNRAS*, 359, 345
- Zu, Y., Kochanek, C. S., Kozłowski, S., & Udalski, A. 2013, *ApJ*, 765, 106

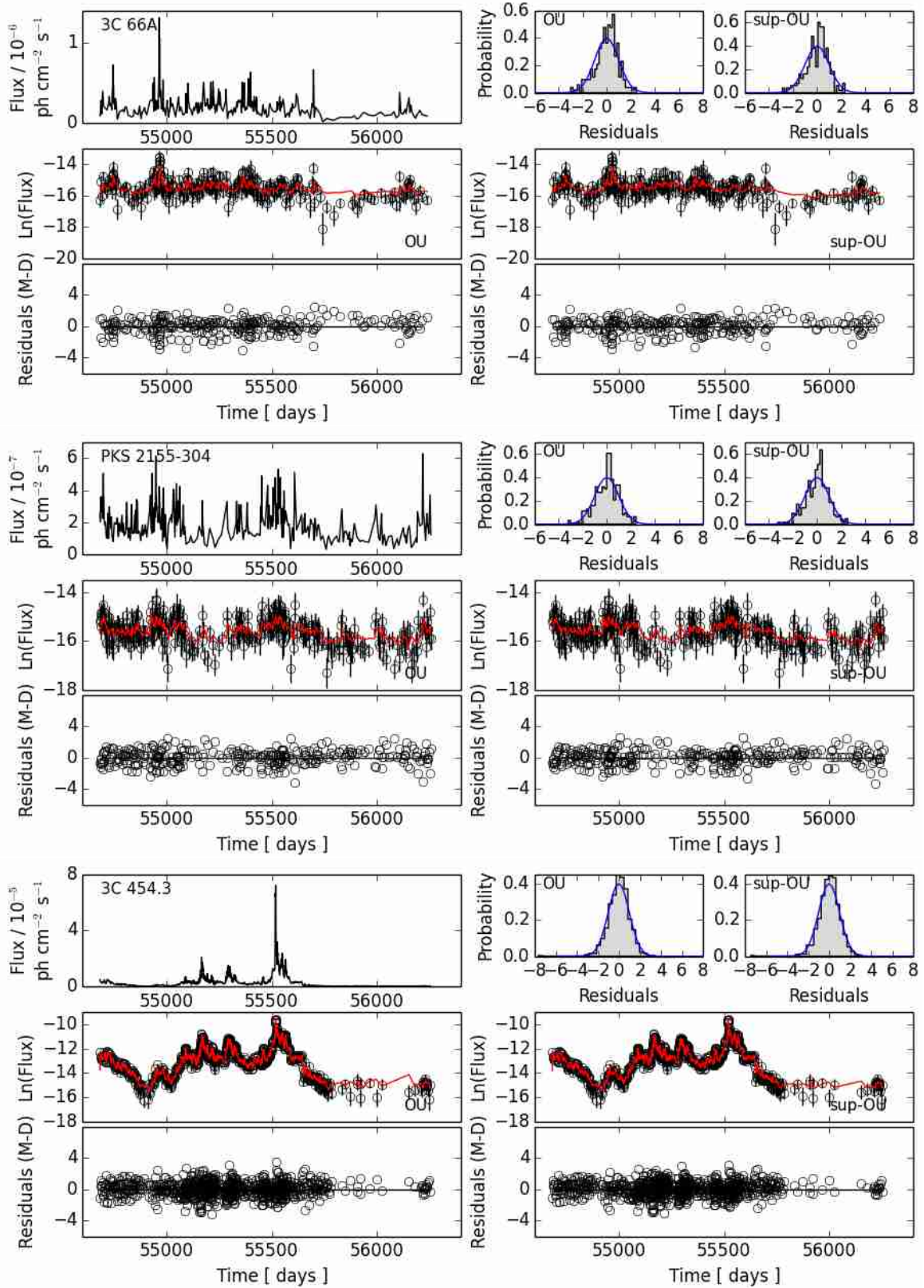


FIG. 2.— Results of modeling for 3C 66A, PKS 2155-304, and 3C 454.3. The sub-panels show for each source the Fermi/LAT light curves (top left); natural logarithm of the light curves, the OU/sup-OU model corresponding to the highest posterior likelihood, and the model standardized residuals (bottom left/bottom right); the histograms of the standardized residuals compared to the expected standard normal distribution (top right). Neither model can be favored based on DIC ( $\Delta\text{DIC} < 10$  in each source).

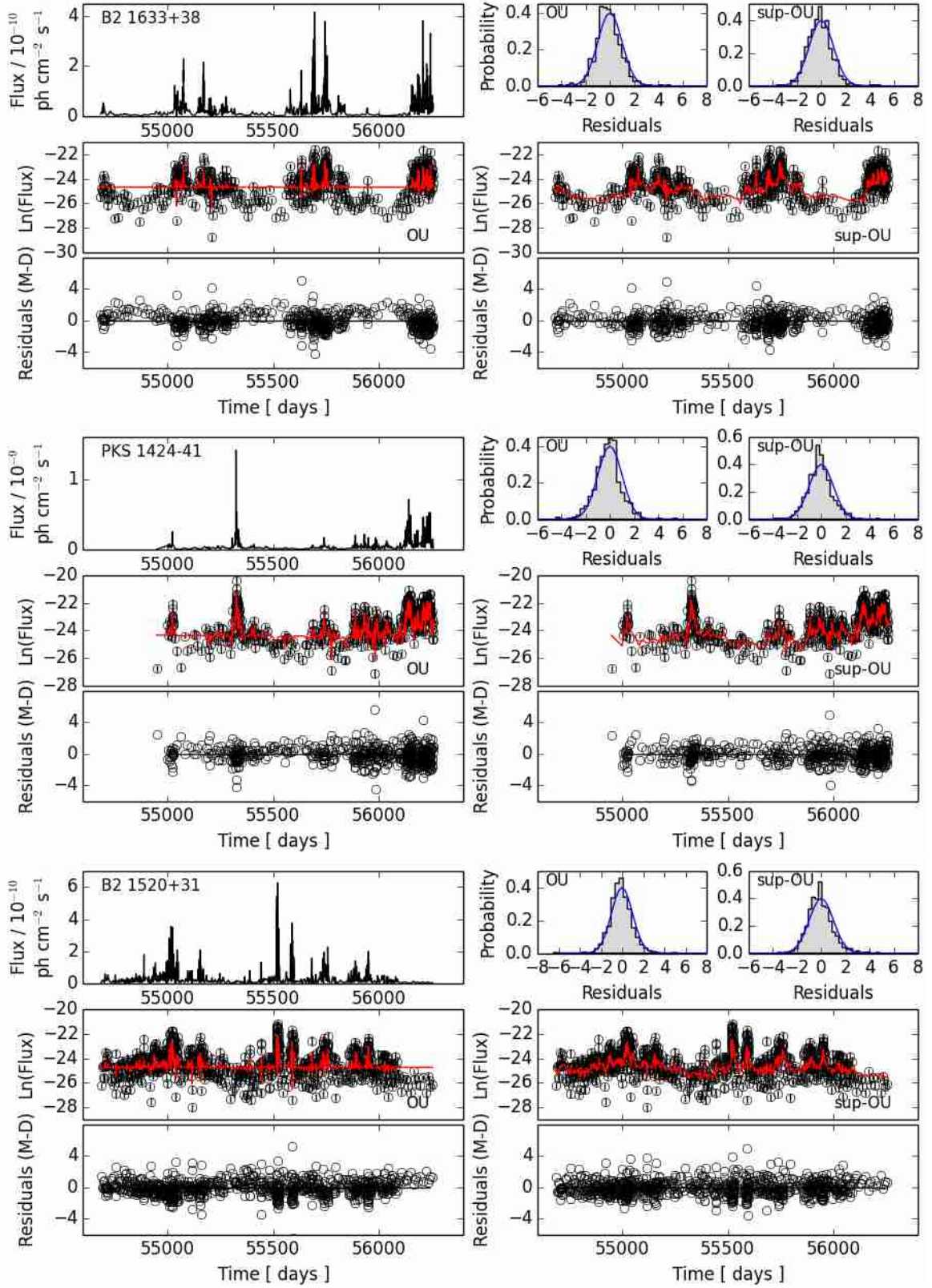


FIG. 3.— Same as Figure 2 for B2 1633+38, PKS 1424-41 and B2 1520+31. The sup-OU model is favored based on DIC ( $\Delta$ DIC  $>$  10).

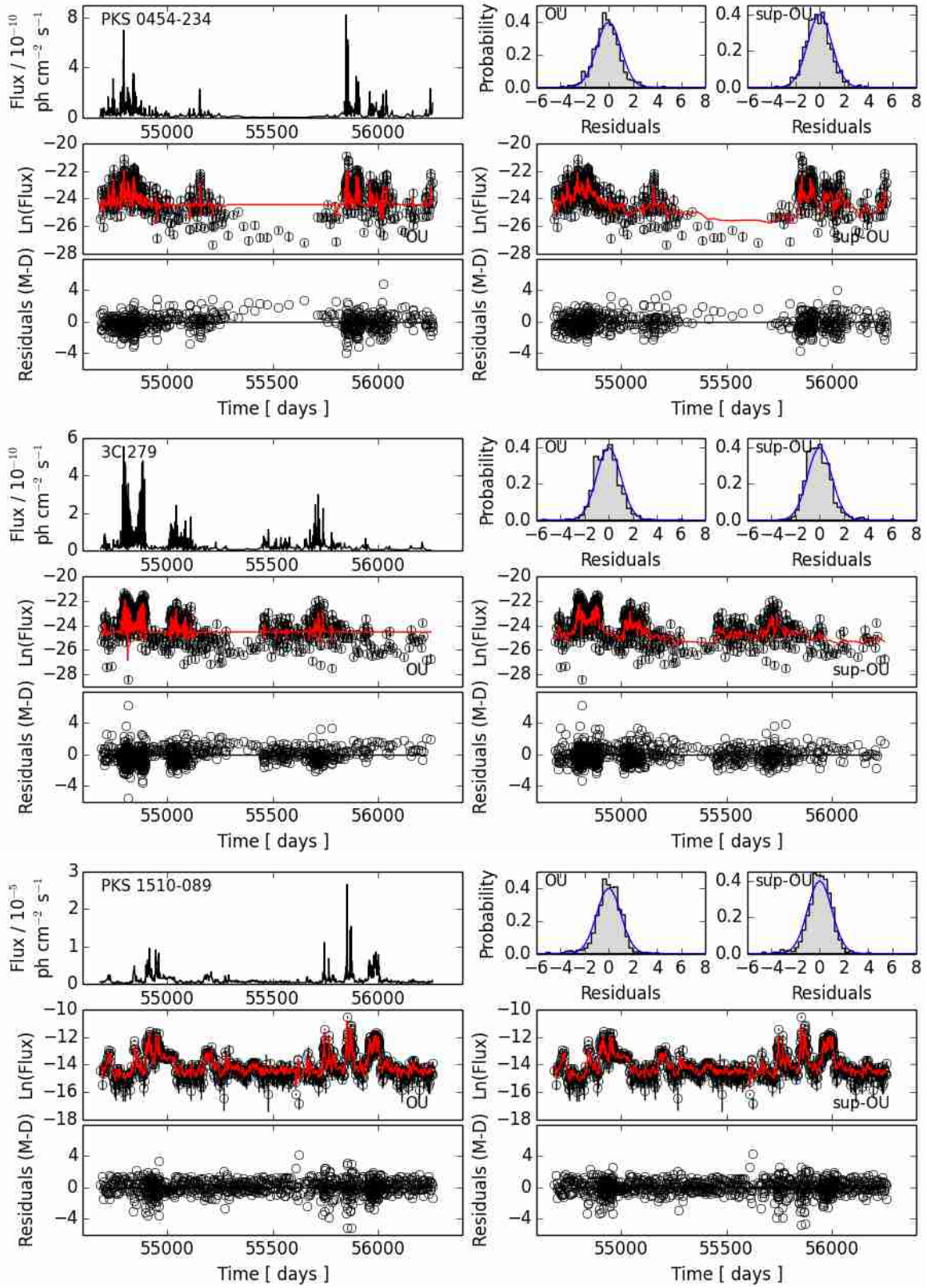


FIG. 4.— Same as Figure 2 for PKS 0454-234, 3C 279 and PKS 1510-089. The sup-OU model is favored based on DIC ( $\Delta\text{DIC} > 10$ ).

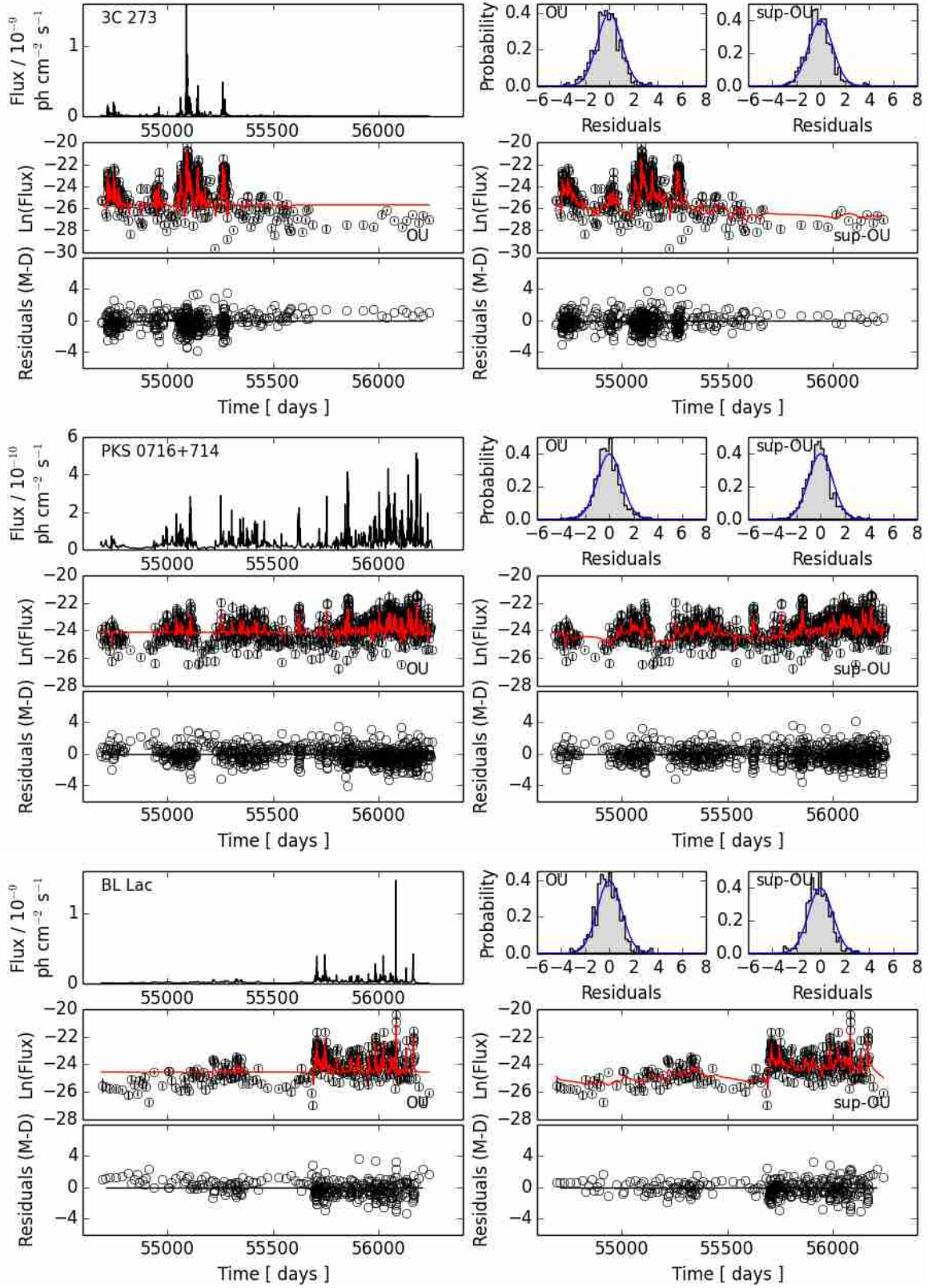


FIG. 5.— Same as Figure 2 for 3C 273, PKS 0716+714 and BL Lac. The sup-OU model is favored based on DIC ( $\Delta\text{DIC} > 10$ ).

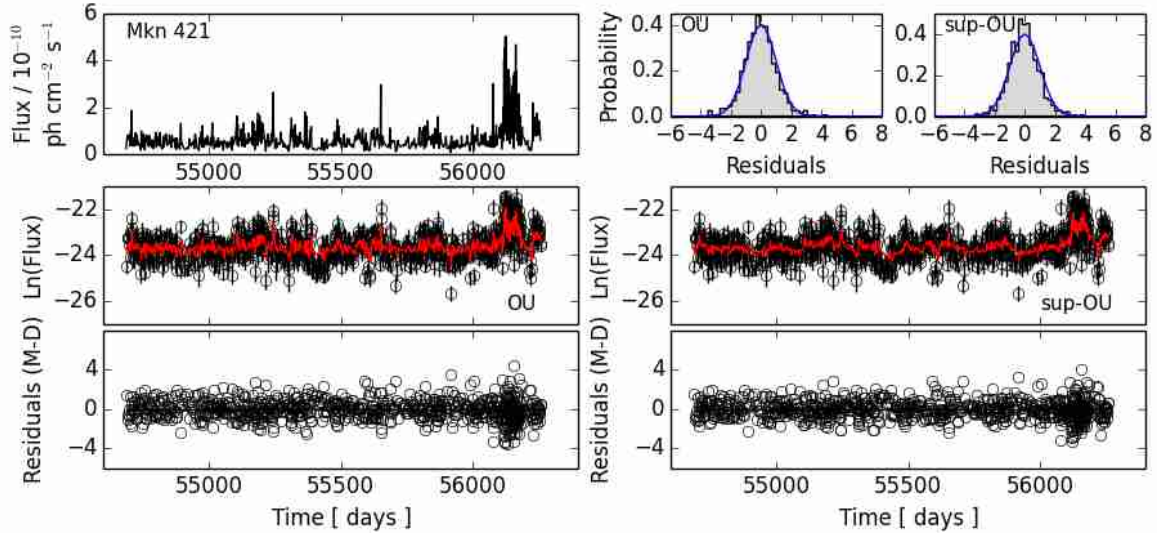


FIG. 6.— Same as Figure 2 for Mkn 421. The sup-OU model is favored based on DIC ( $\Delta\text{DIC} > 10$ ).

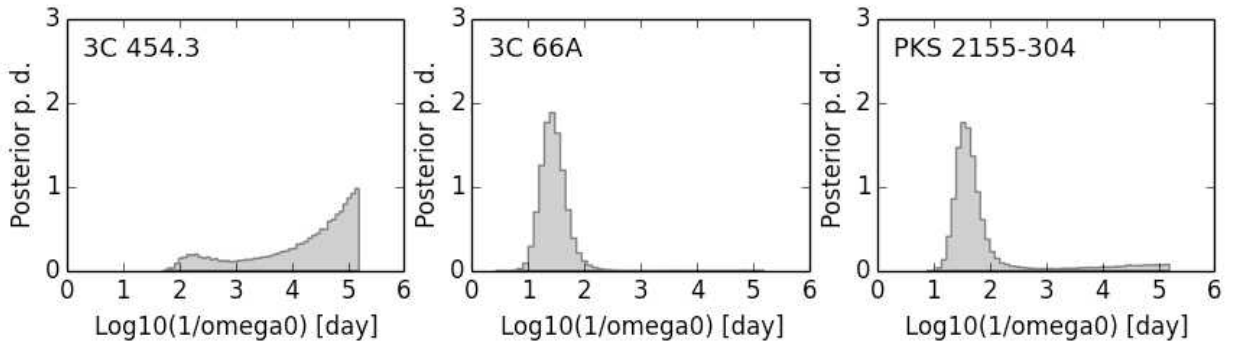


FIG. 7.— Posterior probability distributions of the logarithm of the characteristic time scale,  $\tau_0 = 1/\omega_0$ , resulting from application of the OU process to the Fermi/LAT light curves of 3C 454.3, 3C 66A, and PKS 2155-304.

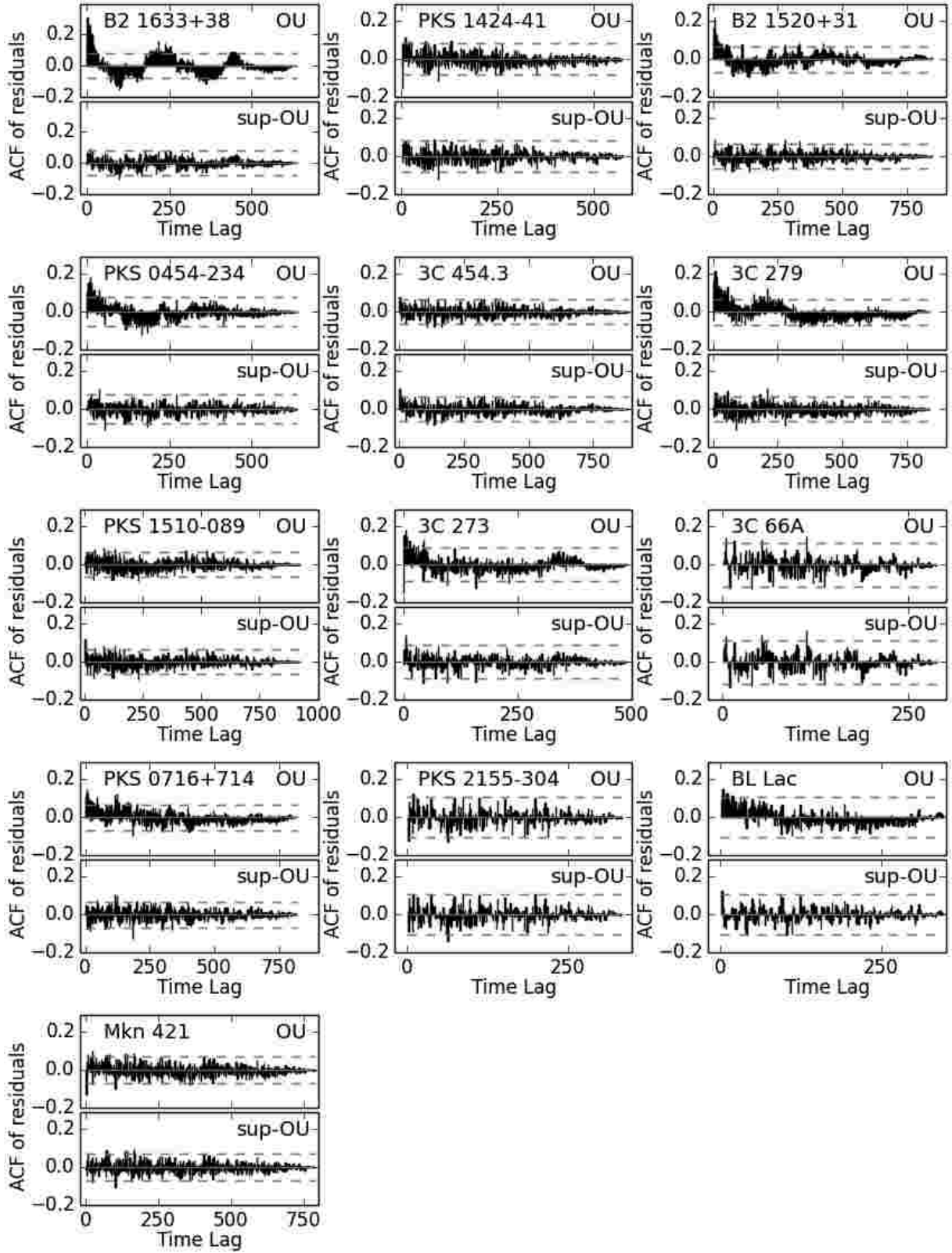


FIG. 8.— Auto-correlation function of the standardized residuals in the OU and sup-OU models. The value at lag 0 is not plotted. The dashed lines represent the 95% confidence limit on the auto-correlation function assuming the white noise process.

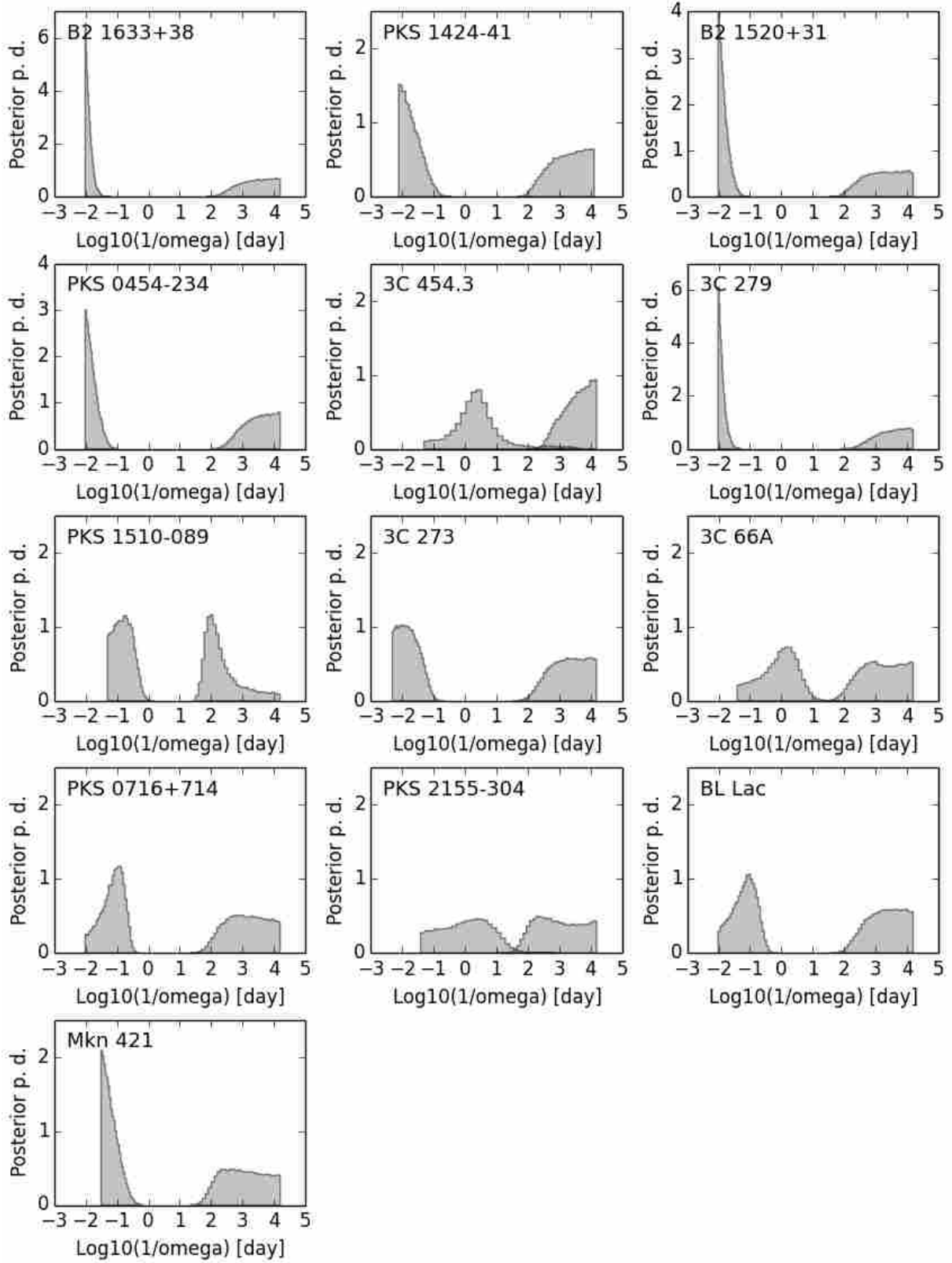


FIG. 9.— Collection of the posterior probability distributions of the logarithm of the short and long characteristic time scales resulting from application of the sup-OU process to the Fermi/LAT light curves.

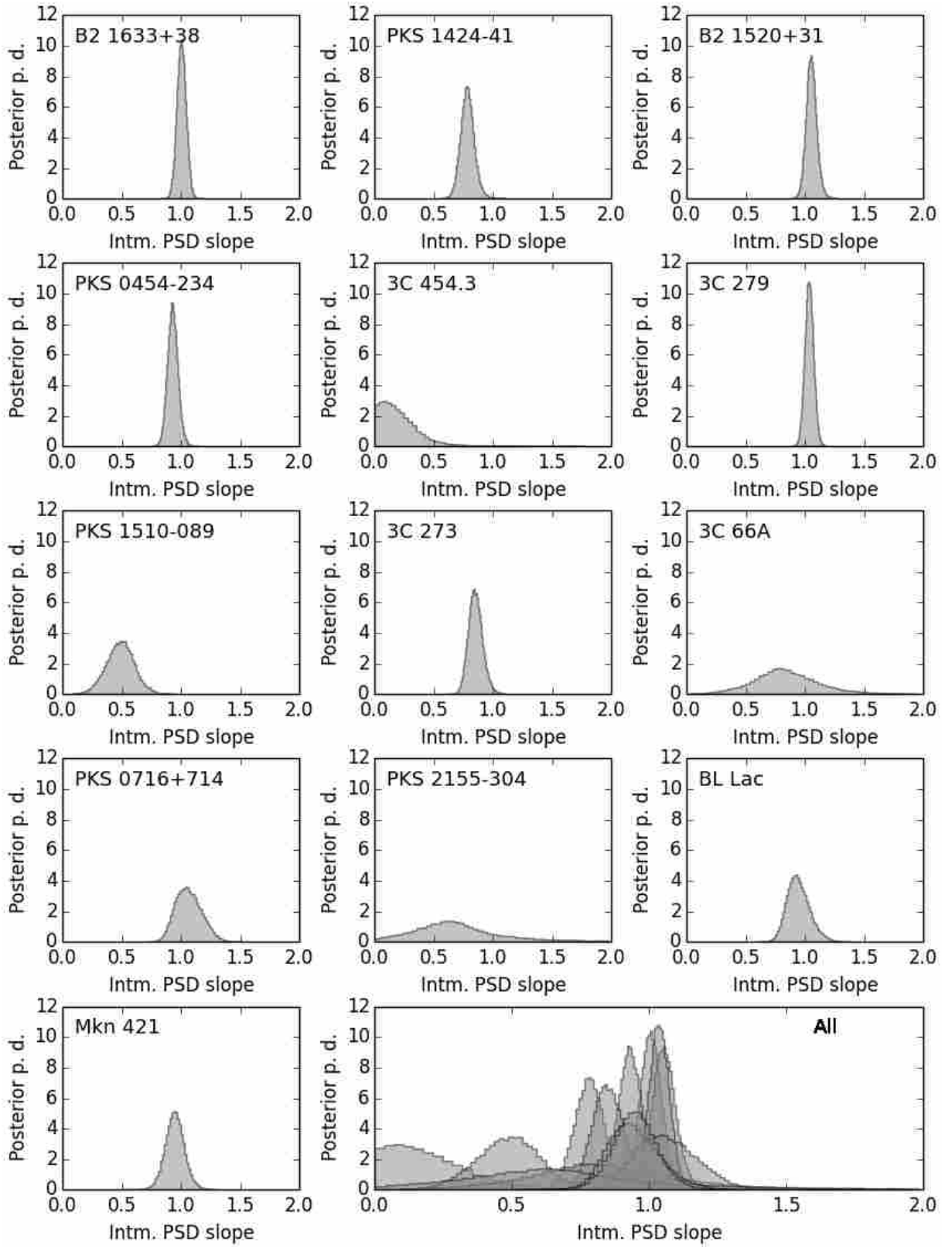


FIG. 10.— Collection of the posterior probability distributions of the intermediate PSD slope,  $\alpha$ , resulting from the application of the sup-OU process to the Fermi/LAT light curves. The bottom-right panel compares distributions of all sources.

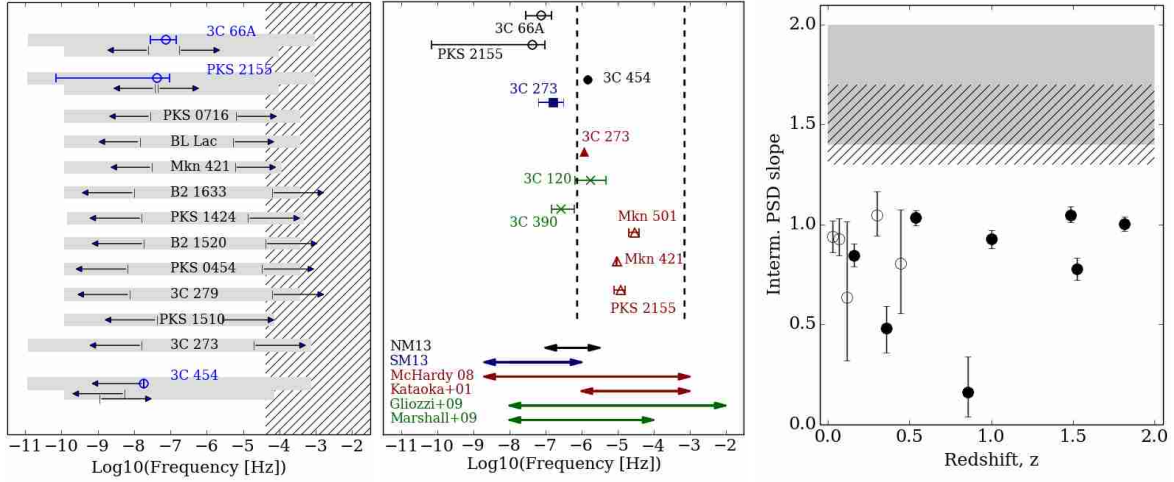


FIG. 11.— Left: Constraints on the characteristic time scales in the Fermi/LAT blazar light curves modeled with our stochastic approach (99% confidence regions in the case of the limits, 90% confidence regions otherwise). Gray horizontal rectangles indicate the range of sampled frequencies. The hatched area marks the frequencies corresponding to sub-hour time scales,  $\tau < 1$  hr. In the case of 3C 66A, PKS 2155-304, and 3C 454.3 results of both the OU and sup-OU modeling are shown; the open circles indicate the OU model constraints. Middle: Compilation of the blazar characteristic time scales across different energy bands from the literature. Open symbols – BL Lac sources, filled symbols – FSRQ sources; triangles – soft X-rays, squares – hard X-rays, circles –  $\gamma$ -rays, open circles – this work; vertical dashed lines – range of  $\tau_S$  detected in the radio-quiet Seyfert galaxies in soft X-rays (Kelly et al. 2011); crosses – detections of soft X-ray  $\tau_S$  in radio-loud AGN. Arrows show the range of frequencies sampled by Kataoka et al. (2001; PKS 2155-304, Mkn 421, Mkn 501), Gliozzi et al. (2009; 3C 390.3), Marshall et al. (2009; 3C 120), McHardy (2008; 3C 273, no error bars provided), Shimizu & Mushotzky (2013; 3C 273), NM13 (3C 454.3, no error bars provided). Right: Intermediate PSD slope as a function of redshift (filled circles - FSRQs, open circles - BL Lacs). The error bars represent the 68% ( $1\sigma$ ) confidence intervals. The hatched and solid rectangles mark the  $1\sigma$  confidence limits on the average PSD slopes in BL Lac and FSRQ sources, respectively (Abdo et al. 2010).